CORROSION SCIENCE AND TECHNOLOGY, Vol.24, No.6(2025), pp.453~469 pISSN 1598-6462 / eISSN 2288-6524
[Research Paper] DOI: https://doi.org/10.14773/cst.2025.24.6.453

Effect of Sulfuric Acid Concentration on Corrosion Between Au or Cu Bonding Wire and Pads for Semiconductor Packaging

Sang-Shin Lee[1], Young-Ran Yoo[2], Seung-Heon Choi[1], Jae-Hyeok Choi[1], Hyeun-Sik Jang[1,3], Young-Cheon Kim[1,3,†], and Young-Sik Kim[3]

[1]*Department of Materials Science and Engineering, Gyeongkuk National University, 1375 Gyeongdong-ro, Andong, Gyeongbuk 36729, Republic of Korea*
[2]*Department of Semiconductor Equipment, Gumi Campus of Korea Polytechnic, 84 Suchul-daero 3-gil, Gumi, Gyeongbuk 39377, Republic of Korea*
[3]*Materials Research Centre for Energy and Clean Technology, Gyeongkuk National University, 1375 Gyeongdong-ro, Andong, Gyeongbuk, 36729, Republic of Korea*

(Received December 10, 2025; Revised December 19, 2025; Accepted December 19, 2025)

Wire bonding is still prevalent in conventional semiconductor packaging. However, degradation can occur during use or storage due to factors such as humidity, acidity, and ionic contamination. This study investigates the corrosion behavior of packaging structures with Al and Au bond pads combined with Au and Cu wires in sulfate-based environments. Electrochemical evaluations, including individual polarization and galvanic tests, were performed in de-aerated 1% Na_2SO_4 solutions with varying H_2SO_4 concentrations. Tafel analysis provided data on corrosion potential (E_{corr}), corrosion current density (i_{corr}), galvanic potential/current density, and total charge. Additionally, a Temperature-Humidity Test (85 °C/85% RH) was conducted under 1% Na_2SO_4 with either 0% or 1% H_2SO_4 conditions, using PCB unit specimens that featured a 1st ball bond on an Al pad and a 2nd stitch bond on an Au pad, bonded with either Au or Cu wires. The surface morphology and elemental distribution were qualitatively analyzed before and after exposure using a 3D optical microscope and FE-SEM/EDS.

Keywords: *Packaging, Au or Cu wire bonding, Al or Au pad, Corrosion, Temperature-Humidity Test*

1. Introduction

The semiconductor manufacturing process typically proceeds in the following order: wafer fabrication, oxide film formation, photolithography and etching, thin-film deposition, ion implantation, metallization, electrical testing, and packaging. In the final packaging stage, the chip is electrically connected to a substrate or lead frame and protected from the external environment. Electrical interconnection methods include wire bonding, flip-chip, solder bonding, through-silicon vias, controlled collapse chip connection, tape-automated bonding, and hybrid bonding. However, wire bonding is still widely used in general-purpose applications because of its process simplicity, cost competitiveness, and compatibility with existing assembly lines [1-4].

The metal wires widely used in wire bonding primarily consist of pure metals such as Au, Cu, and Ag [3]. In addition, alloy systems (e.g., Cu-Pd, Au-Pd, Ag-Pd, Ag-Au) and coated wire systems (e.g., Pd-coated Cu, ultra-thin barrier layers) are employed to improve processability, corrosion resistance, and mechanical properties [2,5,6]. Au wire is widely used because it provides stable bondability and a wide process window [7,8]. Interfacial evolution after bonding (including phase formation and voiding) may affect long-term reliability depending on thermal history and storage conditions [9-11]. Although Cu wire is widely adopted because of its low electrical resistance, high mechanical strength, and cost advantages [12,13], For Cu wire, the interfacial phase distribution and its sensitivity to environmental contaminants (e.g., halides and sulfur species) should be considered in reliability design [14]. These bonding wires are widely used, ranging from round wires for fine-pitch

†Corresponding author: kimyc@gknu.ac.kr
S. S. Lee: Master's degree student, J. H. Choi: Master's degree student, S. H. Choi: Ph.D. candidate, Y. R. Yoo: Professor, H. S. Jang: Professor, Y. C. Kim: Professor, Y. S. Kim: Emeritus

applications (15-30 μm) to aluminum flat wires used for power and automotive wedge bonding. Material selection is determined by a combination of electrical requirements (resistance, high-frequency loss), bonding process tolerances (pressure, time, temperature, etc.), oxidation sensitivity, susceptibility to galvanic corrosion, and cost [3]. Therefore, to ensure reliable package performance, wires with superior corrosion resistance and bonding reliability must be used. In the automotive sector, increasing vehicle electrification has made corrosion resistance and reliability design that account for wide operating temperatures, long service lifetimes, and exposure to chemical contaminants even more important [15-18].

Electrical connections in packages can be exposed to moisture, increased acidity, and ionic contamination during use and storage, resulting in various forms of degradation, including galvanic corrosion, creep corrosion, oxidation and sulfation reactions, halogen-induced pitting, and stress corrosion cracking (SCC) [19-23]. These reactions are influenced by several factors, including the bond pad-bonding wire interface structure, surface film properties, electrolyte composition, and position-dependent current distribution. In particular, the type and distribution of interfacial IMCs (e.g., Au-Al, Cu-Al IMCs) and potential difference are key factors that determine the galvanic current path and the location of local damage (ball neck, heel, and stitch) [24]. Among these, chloride (Cl^-)-containing environments have been the most extensively studied. It has been repeatedly reported that Al pad dissolution and pitting are accelerated with increasing HCl concentration, and that in Cu-Al systems the extent of degradation increases as the level of halogen contamination rises [25-29].

Meanwhile, the ingress pathways of sulfur (S) can be divided into intrinsic and extrinsic. In the intrinsic pathway, internal ingress of S-containing species has been observed in encapsulated leadframe systems [33,34], and ion migration within the epoxy molding compound (EMC) as well as access through crevices (micro-gaps) at the package edge have been reported [12,31,32]. In addition, sulfur species in molding compounds have been discussed as an important factor affecting the high-temperature reliability of Cu–Al wirebond interconnects [30]. Additionally, the application of sulfonate (e.g., MSA)-based electrolyte baths in some plating processes has been reported, raising the possibility of process-origin S residue and contamination [31]. Externally, it has been quantitatively reported that atmospheric SO_2/H_2S significantly increases the atmospheric corrosion rate of Cu by acidifying the wet film, and a synergistic effect is also observed in mixed contamination (e.g., simultaneous presence of $SO_2 + H_2S$ and O_3) [21,22]. In particular, degradation of Cu interconnect properties has been reported upon exposure to H_2S, and deterioration of electrical, thermal, and mechanical properties has also been confirmed in H_2S aging studies of sintered nano-Cu systems, although the systems and environments differ from those considered here [23].

Thus, it is important to establish an experimental concentration range that encompasses the acidity that sulfate-based contamination can actually form when sulfur (S) infiltrates. Cases where significant levels of sulfate (SO_4^{2-}) remain have been reported in field failure and contamination analyses of actual electronic and semiconductor systems, for example, an IC/MS-based case study identified SO_4^{2-} residuals in the affected area in the range of 51.93 μg/in^2 ~ 559.85 μg/in^2 (i.e., 8.05 μg/cm^2 to 86.78 μg/cm^2) [50]. However, direct conversion of these residuals to H_2SO_4 concentration (wt%) requires assumptions about the amount (thickness) of the water film involved in dissolution, making it difficult to accurately convert them considering actual environmental variability. Therefore, in this study, we cover the range of mild to strong acidity, where in the literature Al alloys are evaluated at approximately 0.98 wt% to 9.81 wt% H_2SO_4 [51] and Cu is evaluated at approximately 4.9 wt% H_2SO_4 [52].

As summarized above, field contamination and sulfur-containing environments generated during the manufacturing process act as important variables for the packaging reliability of semiconductor packages. To systematically evaluate these environmental influences, this study set a range of sulfuric acid concentrations (0 wt%, 0.1 wt%, 1 wt%, and 10 wt%) and stepwise constructed a low-acid reference condition (1 wt% Na_2SO_4), actual acidity candidate conditions (1 wt% Na_2SO_4 + 0.1 wt% and 1 wt% H_2SO_4), and a strong acid condition (1 wt% Na_2SO_4 + 10 wt% H_2SO_4). Based on these conditions, this study evaluated the galvanic corrosion behavior of pads (aluminum or gold) bonded with gold or copper wires in a sulfuric acid (H_2SO_4)

environment and analyzed the electrochemical factors affecting the behavior. Furthermore, to verify reliability behavior in environments similar to actual use conditions, a device similar to the product was fabricated and temperature-humidity testing (THT) was performed. Through this, the corrosion behavior observed at the first ball joint and the second stitch joint was compared with the electrochemical evaluation results to interpret the results and elucidate the joint vulnerability mechanism in a sulfuric acid environment.

2. Experimental methods

2.1 Materials

2.1.1 Specimens for electrochemical test

High-purity Al (99.999%) was deposited on a 4-inch Si wafer using a DC magnetron sputtering system (KVS-2002L, Korea Vacuum Tech, Kimpo, Korea) to form a bond-pad thin film, at a power of 50 W with an Ar flow rate of 20 sccm and a pressure of 1 mTorr. The thickness of the Al thin film was approximately 605 nm. The bonding wires used were Au and Cu wires with a diameter of 25 μm. The wires were manufactured by MK Electron Co., Ltd. (Yongin, Korea) using a continuous casting-sintering process, followed by heat treatment and winding to obtain a final diameter of 25 μm. The wires were attached to copper leads using carbon tape to define the electrical connection and the exposed working area for electrochemical testing. All regions except the exposed area (0.04 cm^2) were insulated with epoxy.

2.1.2 Specimens for temperature and humidity test

A PCB unit for reliability evaluation was fabricated by wire bonding on the bond pads of an FR-4 PCB using a K&S RAPID PRO bonder (Kulicke & Soffa, Singapore) [34]. The first ball bond was formed on a pure Al pad using either Au or Cu wire with a diameter of 25 μm. The thickness of the Al pad was 10,000 Å - 12,000 Å (≈1.0 μm - 1.2 μm). The second stitch bond was then formed on a pure Au pad using wire of the same diameter. The thickness of the Au pad was 0.3 μm. The detailed bonding conditions are presented in Table 1. The fabrication was performed by MK Electron Co., Ltd. (Yongin, Korea).

2.2 Polarization test

A three-electrode cell experiment was conducted using Au wire, Cu wire, and sputtered Al as working electrodes, a Pt wire as the counter electrode, and a saturated calomel electrode (SCE) as the reference electrode. The electrolyte consisted of 1% Na_2SO_4 with H_2SO_4 concentrations of 0%, 0.1%, 1%, and 10%. All tests were performed at 25 °C, and the solutions were degassed with N_2 at a flow rate of 200 mL/min for 30 min prior to testing. A potentiostat (Interface 1000, Gamry, Warminster, PA, USA) was used. Prior to polarization, potentiostatic conditioning was performed at –0.2 V(SCE) for 60 s with respect to the corrosion potential. After an additional stabilization period of 150 s, polarization tests were carried out at a scan rate of 0.33 mV/s [35]. The polarization starting potential was adjusted for each condition, and the corrosion rate was calculated according to ASTM G102 after the test [36]. Based on the electromotive force (EMF) series, sputtered Al was treated as the anodic material and Au and Cu wires as cathodic materials. Accordingly, the anodic Tafel slope was obtained from the polarization curves of sputtered Al, while the cathodic Tafel slopes were obtained from those of the Au and Cu wires [37].

2.3 Electrochemical galvanic test

When the bonding wire is joined to the Al pad, dissimilar metals are brought into contact. Therefore, galvanic corrosion behavior was evaluated by electrochemical galvanic testing [38]. The reference

Table 1. Wire bonding conditions

	Au wire			Cu wire		
	1st Ball bond	2nd Stitch bond	*EFO	1st Ball bond	2nd Stitch bond	*EFO
Current (mA)	80	100	30	55 ~ 85	75 ~ 120	40
Time (μs)	15	15	700	5 ~ 10	10	730
Force (grams)	30	60	-	25 ~ 70	45 ~ 75	-

*EFO: Electronic Flame-Off

electrode was a saturated calomel electrode (SCE). The test electrode (anode) was the Al pad, and the counter electrode (cathode) was the bonding wire. The effective anode-to-cathode area ratio was set to 1:1. The electrolyte was 1% Na_2SO_4 containing 0, 0.1, 1, or 10% H_2SO_4. Galvanic tests were performed using a potentiostat (Interface 1000, Gamry, Warminster, PA, USA), and the galvanic potential and current density were continuously monitored during the test. The average corrosion current density (i_{corr}) was calculated from the accumulated charge using Equation (1), and the corrosion rate was calculated in accordance with ASTM G102 [36].

$$i_{corr}\left(\frac{A}{cm^2}\right) = \frac{Q\left(\frac{C}{cm^2}\right)}{\Delta t(s)} \tag{1}$$

2.4 Temperature-Humidity Test

For the unit specimen, a THT was performed at 85 °C and 85% RH using a PR-2J chamber (ESPEC, Osaka, Japan) [18]. A 1% Na_2SO_4 solution and a 1% Na_2SO_4 + 1% H_2SO_4 solution were used as test electrolytes in a 1 L beaker fixed inside the test chamber. During the test, the unit specimen was fixed vertically in epoxy to avoid direct contact with the solution [19]. PCB specimens underwent experiments at 10 h, 100 h, and 1000 h, respectively, and changes in surface morphology and element distribution were analyzed. A 3D microscope (VK-X3000, Keyence, Itasca, IL, USA) was used to observe the surfaces of the 1st ball bond, 2nd stitch bond, and wire. FE-SEM (MIRA3, TESCAN, Brno, Czech Republic) and EDS (energy-dispersive X-ray spectrometer, Mmax 50, Oxford, UK) were used to characterize the surface morphology and elemental distribution of the specimens before the test, as well as changes in the morphology of corrosion products and local damage after THT.

3. Results and Discussion

3.1 Electrochemical corrosion of Au, Cu bonding wire, and Al pad

Fig. 1 shows the effect of sulfuric acid concentration on the polarization behavior of sputtered Al, Au wire, and Cu wire in 1% Na_2SO_4 solution. Fig. 1a shows the polarization curve of sputtered Al. As the sulfuric acid

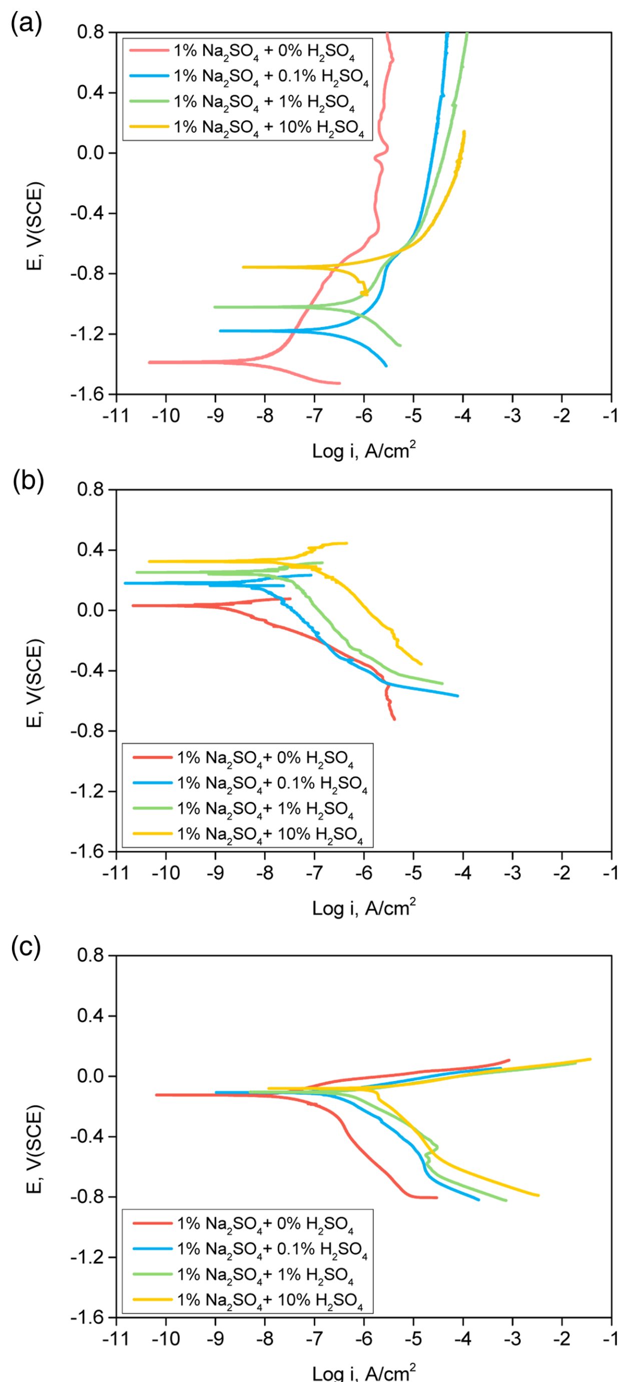

Fig. 1. Effect of sulfuric acid concentration on the polarization curve in deaerated 1% Na_2SO_4 + x% H_2SO_4 at 25 °C: (a) Sputtered Al, (b) Au wire, (c) Cu wire

concentration increases, the corrosion potential (E_{corr}) increases. This result is consistent with previous reports that, in acidic environments, a stable oxide layer thickens to form a passive state and the corrosion potential of Al increases [39]. The corrosion current density (i_{corr}) and the

Table 2. Parameters obtained from polarization test (1% Na_2SO_4 + x% H_2SO_4) at 25 °C

Parameters	H_2SO_4	0%	0.1%	1%	10%
E_{corr}(SCE), mV	Sputtered Al	–1386	–1182	–1017	–758
	Au wire	+31	+180	+ 252	+ 323
	Cu wire	–124	–109	–105	–81
i_{corr}, μA/cm^2	Sputtered Al	+ 0.0034	+ 0.1007	+ 0.1468	+ 0.2550
	Au wire	+ 0.0009	+ 0.0028	+ 0.0118	+ 0.0234
	Cu wire	+ 0.0179	+ 0.2292	+ 0.4450	+ 1.0760
β_a, mV/decade	Sputtered Al	+ 41	+ 43	+ 47	+ 49
β_c, mV/decade	Au wire	–34	–33	–27	–24
	Cu wire	–342	–303	–176	–178

passivation current (i_p) both increase. The anodic Tafel slope (β_a) increases slightly, but the effect is not significant. Fig. 1b shows the polarization curve of the Au wire. As the sulfuric acid concentration increases, the corrosion potential increases, while the change in corrosion current density is very small. This behavior is consistent with (1) the findings of G. Zahed et al. that the hydrogen evolution reaction promoted by acidification mainly increases the cathodic current at that potential and does not directly increase the overall current [48], and (2) the results of B. Saeid et al. that increasing the sulfuric acid concentration during cyclic polarization mainly affects surface roughness and adsorption, without significantly enhancing anodic dissolution [49]. Fig. 1c shows the polarization curves of the Cu wire. With increasing H_2SO_4 concentration, the corrosion potential (E_{corr}) shifts slightly in the noble direction, but the change is not significant. This behavior can be rationalized by established electrochemical principles: (1) according to the E-pH diagram proposed by M. Pourbaix, a decrease in pH thermodynamically favors the dissolution of Cu [42], and (2) as described in Uhlig's Corrosion Handbook, in acidic solutions the increase in the exchange current density of the hydrogen evolution reaction reduces cathodic polarization, thereby allowing larger cathodic currents to flow at a given potential [41]. The polarization parameters obtained from the curves in Fig. 1 are summarized in Table 2.

Fig. 2 shows the corrosion rates calculated from the corrosion current densities obtained from the polarization curves in Fig. 1 using Faraday's law. First, the corrosion rates of sputtered Al are 0.037 μm/y, 1.096 μm/y,

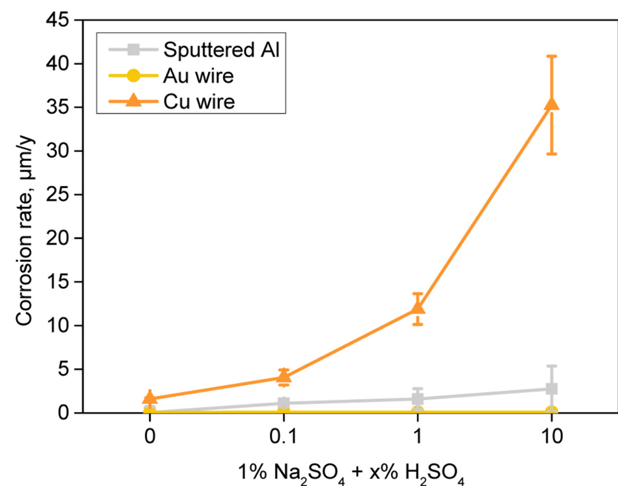

Fig. 2. Effect of sulfuric acid concentration on the corrosion rate of sputtered Al, Au wire, and Cu wire in deaerated 1% Na_2SO_4 + x% H_2SO_4 obtained from Fig. 1

1.59 μm/y, and 2.77 μm/y, increasing gradually with increasing sulfuric acid concentration. This trend can be explained as follows: (1) W. C. Moshier reported that Al forms a wide passive region in Na_2SO_4 solution and that the passive current remains low even as the potential increases [39], and (2) A. Kolics reported that, even when the sulfate concentration in the solution increases, SO_4^{2-} does not directly break down the film, thereby suppressing any increase in corrosion current and limiting the increase in corrosion rate [40]. Third, although the study by Y. R. Yoo et al. was conducted in a chloride-containing environment, XRD analysis showed that sputtered Al contained partially amorphous regions and exhibited a lower corrosion rate than bulk Al [27]. The corrosion rates of the Au wire were 0.066 μm/y, 0.11 μm/y, 0.11 μm/y,

and 0.12 μm/y, indicating that they were not greatly affected by the increase in sulfuric acid concentration. Among the three materials, Au wire exhibited the lowest corrosion rates. By contrast, the corrosion rates of the Cu wire were 1.59 μm/y, 4.08 μm/y, 11.89 μm/y, and 35.25 μm/y. Under 1% Na_2SO_4 conditions, the corrosion rate of Cu wire was about 43 times that of sputtered Al and about 24 times that of Au wire. Under 1% Na_2SO_4 + 10% H_2SO_4 conditions, it was approximately 13 times higher than that of sputtered Al and about 300 times higher than that of Au wire.

Fig. 3 shows the effect of sulfuric acid concentration on the galvanic corrosion behavior measured in 1% Na_2SO_4 + x% H_2SO_4 at 25 ºC, using Au wire as the counter electrode and sputtered Al as the working electrode. Fig. 3a shows the change in galvanic current density with time. The current density increases significantly as the sulfuric acid concentration increases. Fig. 3b shows the change in galvanic potential with time. In general, as the sulfuric acid concentration increases, the galvanic potential of Al shifts to more negative values, and with increasing test time it shifts further in the negative direction.

Fig. 4 shows the effect of sulfuric acid concentration on the galvanic corrosion behavior measured in 1% Na_2SO_4 + x% H_2SO_4 at 25 ºC, with Cu wire as the counter electrode and sputtered Al as the working electrode. Error data caused by surface damage was corrected and fitted to calculate the corrosion rate. Fig. 4a shows the change in galvanic current density with time, and it can be seen that the increase in current is smaller than in Fig. 3a, where Al was connected to Au wire. Fig. 4b shows the change in galvanic potential with time. In general, as the sulfuric acid concentration increases, the galvanic potential of Al shifts to more negative values, and it becomes increasingly negative with test time. When 10% sulfuric acid is added, both the galvanic potential and the galvanic current density change markedly.

Fig. 5 summarizes the single and galvanic corrosion

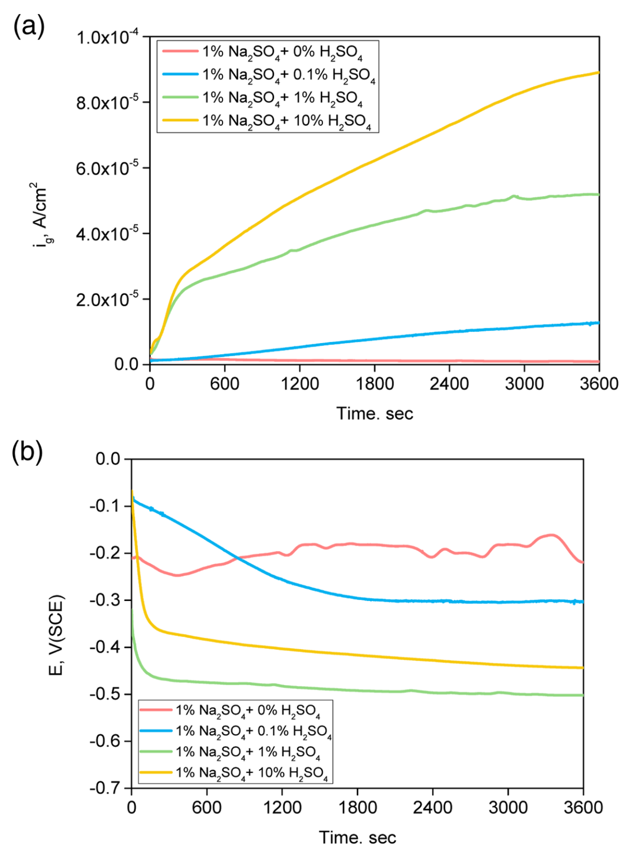

Fig. 3. Effect of sulfuric acid concentration on (a) galvanic current density and (b) galvanic potential of Au wire and sputtered Al couple in deaerated 1% Na_2SO_4 + x% H_2SO_4 at 25 ºC (Working electrode: sputtered Al)

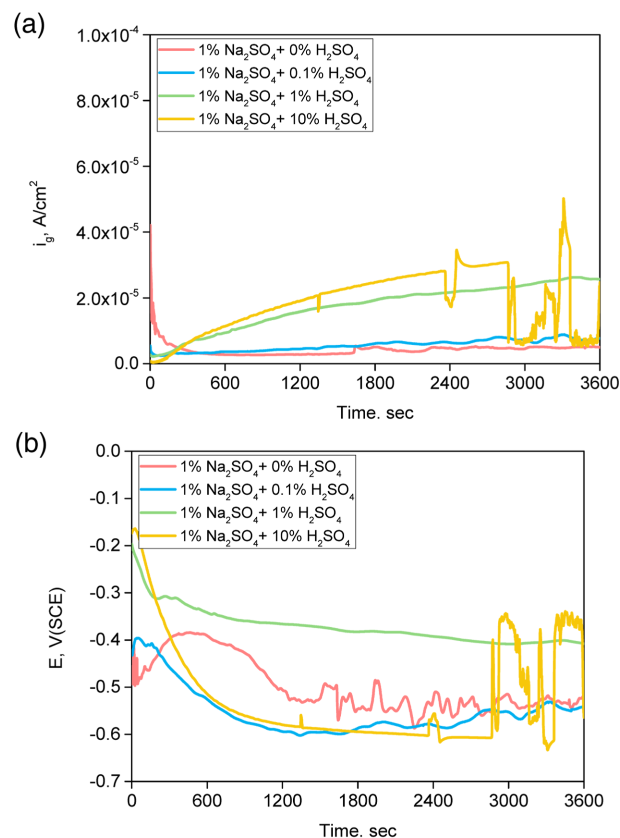

Fig. 4. Effect of sulfuric acid concentration on (a) galvanic current density and (b) galvanic potential of Cu wire and sputtered Al couple in deaerated 1% Na_2SO_4 + x% H_2SO_4 at 25 ºC (Working electrode: sputtered Al)

rates of sputtered Al obtained from Fig. 3 and Fig. 4. Fig. 5a shows the results for the Au-Al galvanic pair. The corrosion rate of the Au-Al couple increases significantly with increasing sulfuric acid concentration compared with the single corrosion rate of sputtered Al. Fig. 5b shows the results for the Cu-Al galvanic pair. Although the corrosion rate of Al increases with increasing sulfuric acid concentration, the increase is smaller than that of the Au-Al galvanic pair. This difference can be explained as follows: (1) Using the individual E_{corr} values in Table 2, the electromotive force (EMF) series referenced to the standard hydrogen electrode (SHE) indicates that ΔE for the Au-Al couple is larger than that for the Cu-Al couple [37]. (2) From the perspective of mixed potential theory, the polarization results in this study show that the cathodic Tafel slope of the Au wire is gentler, resulting in a larger current at the intersection point with the anodic branch of sputtered Al [41]. (3) The hydrogen evolution reaction on

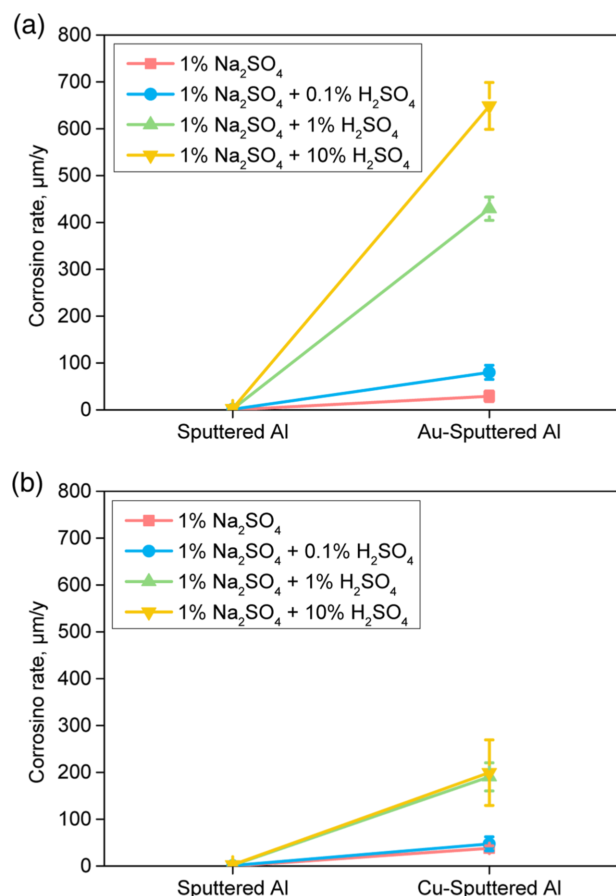

Fig. 5. Effect of galvanic coupling on the corrosion rate obtained from Fig. 4 in deaerated 1% Na_2SO_4 + x% H_2SO_4: (a) Au-Al couple, (b) Cu-Al couple

Au in sulfuric acid solution is enhanced, leading to a larger cathodic current at a given potential and thus a higher current in the Au-Al galvanic couple [48].

3.2 Corrosion appearance of wire-bonded PCB unit specimen by Temperature-Humidity Test

Fig. 6 and Fig. 7 show the changes in external appearance of the unit in which the Au wire is 1st ball bonded on the Al pad and 2nd stitch bonded on the Au pad, after exposure to 1% Na_2SO_4 and 1% Na_2SO_4 + 1% H_2SO_4 solutions for 0 h, 10 h, 100 h, and 1000 h. Fig. 6 presents the surface appearance as a function of exposure time in 1% Na_2SO_4 solution. Up to 10 h, no noticeable change is observed on the surface; however, at 100 h, slight discoloration appears on the Al pad around the ball bond. At 1000 h, this discoloration at the edge of the ball bond remains, but no significant change in the overall morphology is observed. Fig. 7 shows the surface appearance as a function of exposure time in 1% Na_2SO_4 + 1% H_2SO_4 solution. Up to 10 h, there is no pronounced change on the surface, but at 100 h, a slight darkening around the ball bond can be seen. After 1000 h, the discolored region on the Al pad surrounding the ball bond further expands. After the macroscopic observation using a 3D microscope, the surface morphology and elemental distribution in the regions of the 1st ball bond and 2nd stitch bond of each unit were examined by FE-SEM and EDS. Quantitative EDS analyses were performed at specified points. In the initial (0 h) condition, slight local shape changes associated with heating and deformation during bonding are observed at the edge of the 1st ball bond, whereas the cutting mark left by severing the wire is clearly visible in the 2nd stitch bond.

Fig. 8 shows the SEM-EDS elemental mapping and point analysis results for the 1st ball bond of the Au-wired unit. Compared with the initial state (0 h), where the shapes of the Au ball bond and Al pad are clearly defined, no distinct change is observed at 10 h in either 1% Na_2SO_4 or 1% Na_2SO_4 + 1% H_2SO_4. In contrast, clear differences appear after 1000 h. In 1% Na_2SO_4, the Al signal becomes slightly weaker and an O signal begins to appear. In 1% Na_2SO_4 + 1% H_2SO_4, the signals from both Au and Al decrease in intensity, while the O signal becomes pronounced. Consistently, the point analysis results indicate little change up to 10 h under both conditions, whereas after 1000 h the wt% of Au and Al decreases and the wt% of O increases.

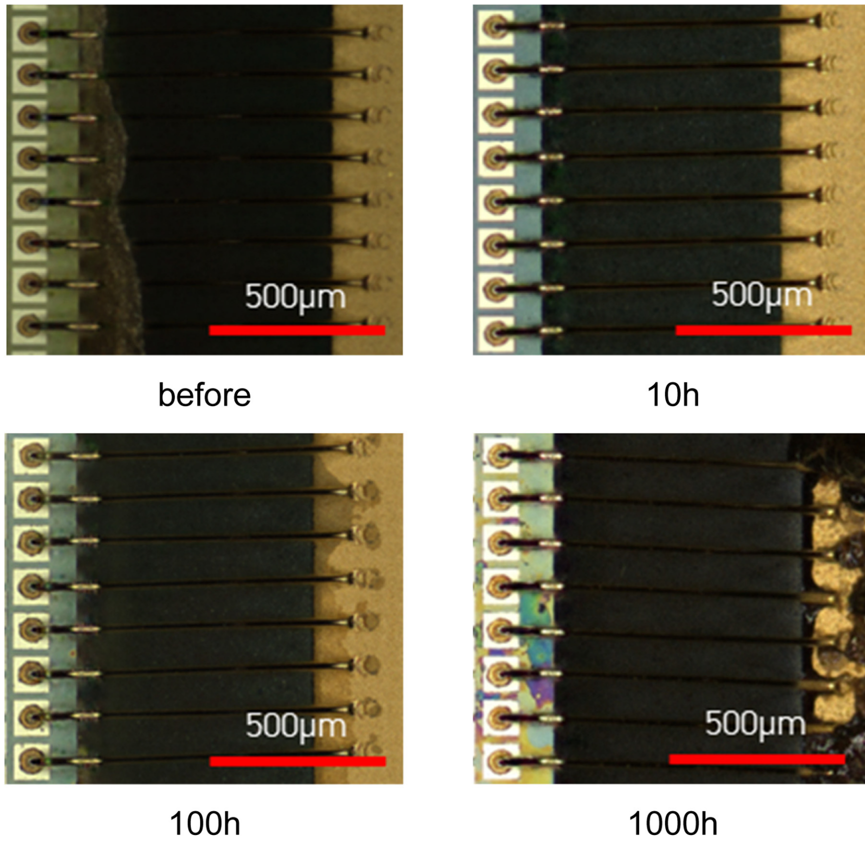

Fig. 6. Effect of test duration on corrosion appearance of Au wire-bonded PCB unit by THT (Test chamber: 85 ºC/85% RH, Test solution in corrosion cell: 1% Na_2SO_4)

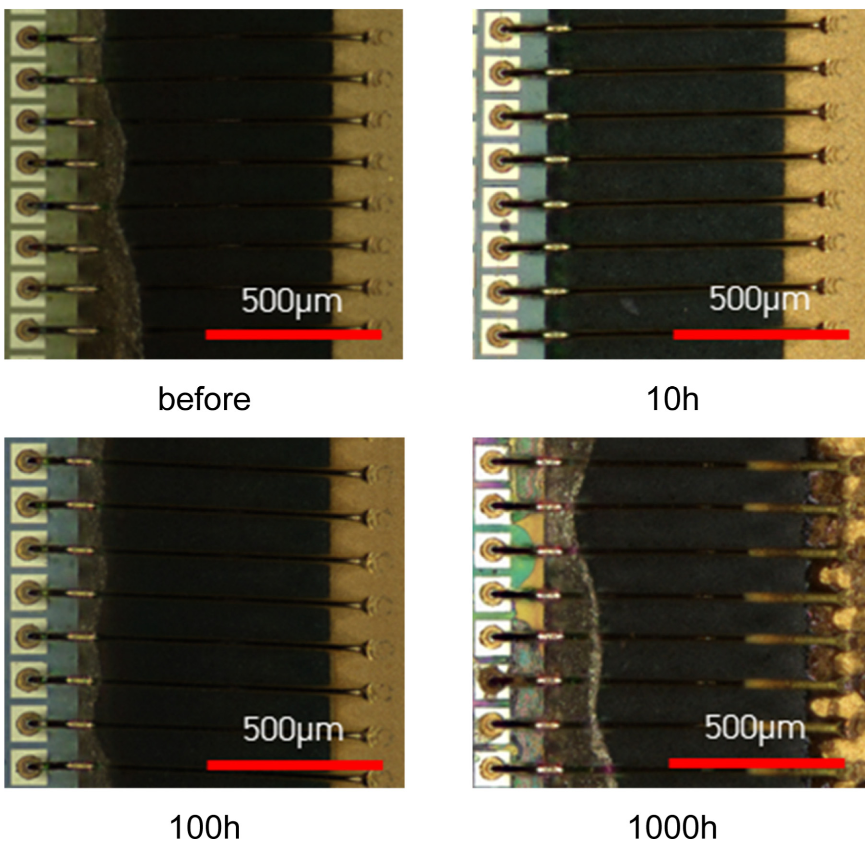

Fig. 7. Effect of test duration on corrosion appearance of Au wire-bonded PCB unit by THT (Test chamber: 85 ºC/85% RH, Test solution in corrosion cell: 1% Na_2SO_4 + 1% H_2SO_4)

Fig. 9 presents the FE-SEM images and EDS results for the 2nd stitch bond of the Au-wired unit. At 0 h, the stitch bond geometry is clearly defined. For both 1% Na_2SO_4 and 1% Na_2SO_4 + 1% H_2SO_4, no noticeable change in appearance is observed, and the morphology is retained up to 10 h. After 1000 h, however, both conditions exhibit a

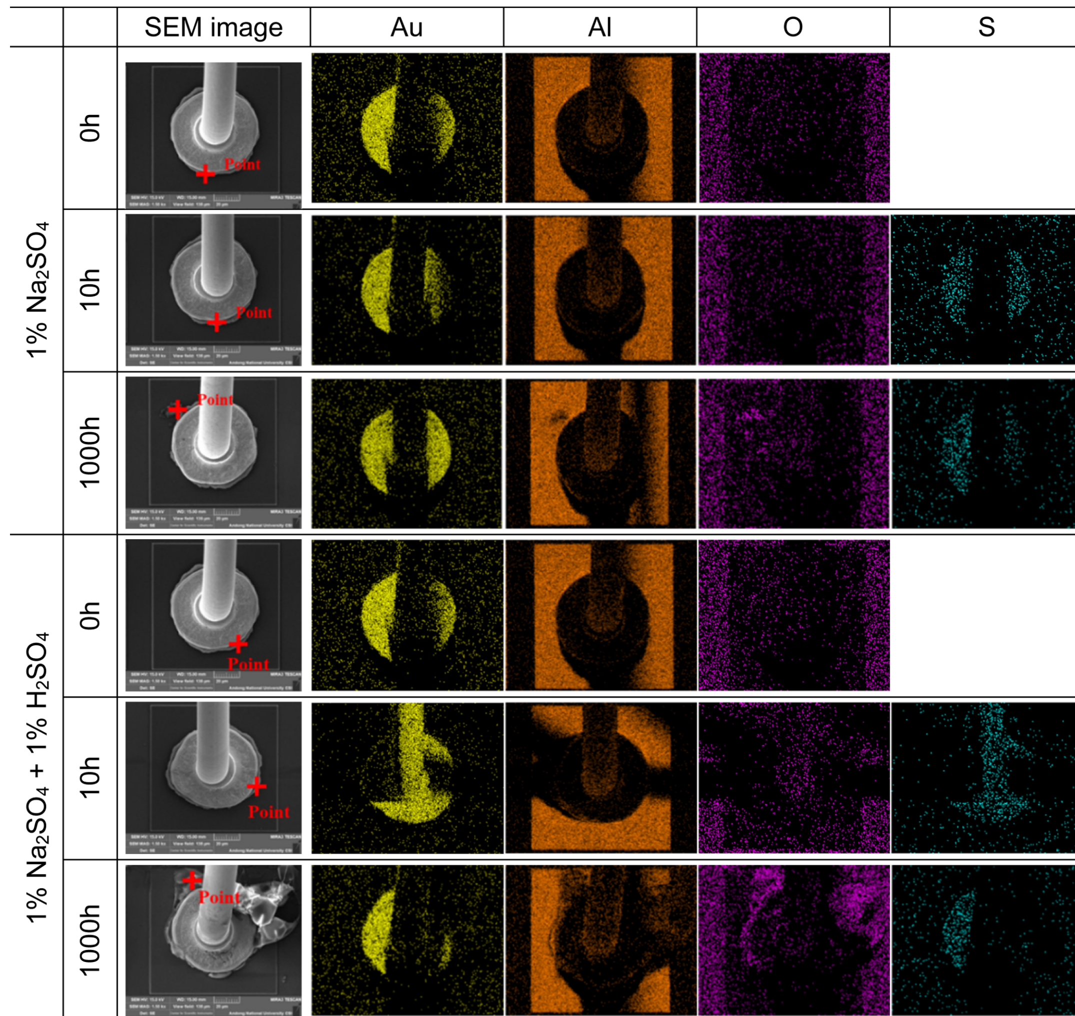

(a)

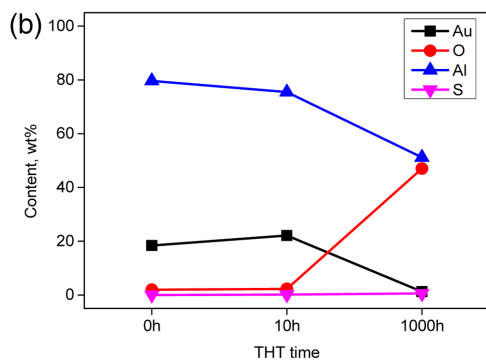

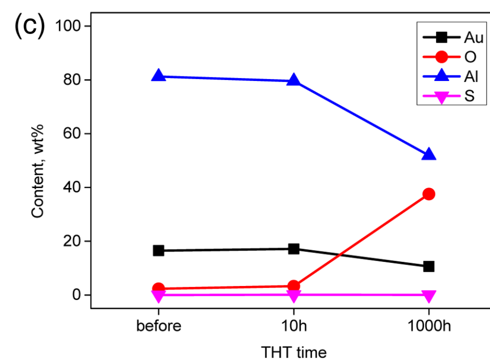

Fig. 8. Elemental distribution of 1st ball bond area of Au wire-bonded PCB unit by THT (Test chamber: 85 °C/85% RH, Test solution in corrosion cell: 1% Na_2SO_4 + x% H_2SO_4): (a) SEM image and EDS mapping, (b) Point analysis for 1% Na_2SO_4, (c) Point analysis for 1% Na_2SO_4 + 1% H_2SO_4

decrease in the signals from the Au wire and Au pad, accompanied by a pronounced increase in the O and Ni signals. The point analysis likewise shows little change up to 10 h, but after 1000 h the Au wt% markedly decreases, while the O and Ni wt% increase significantly. This behavior is consistent with previously reported observations

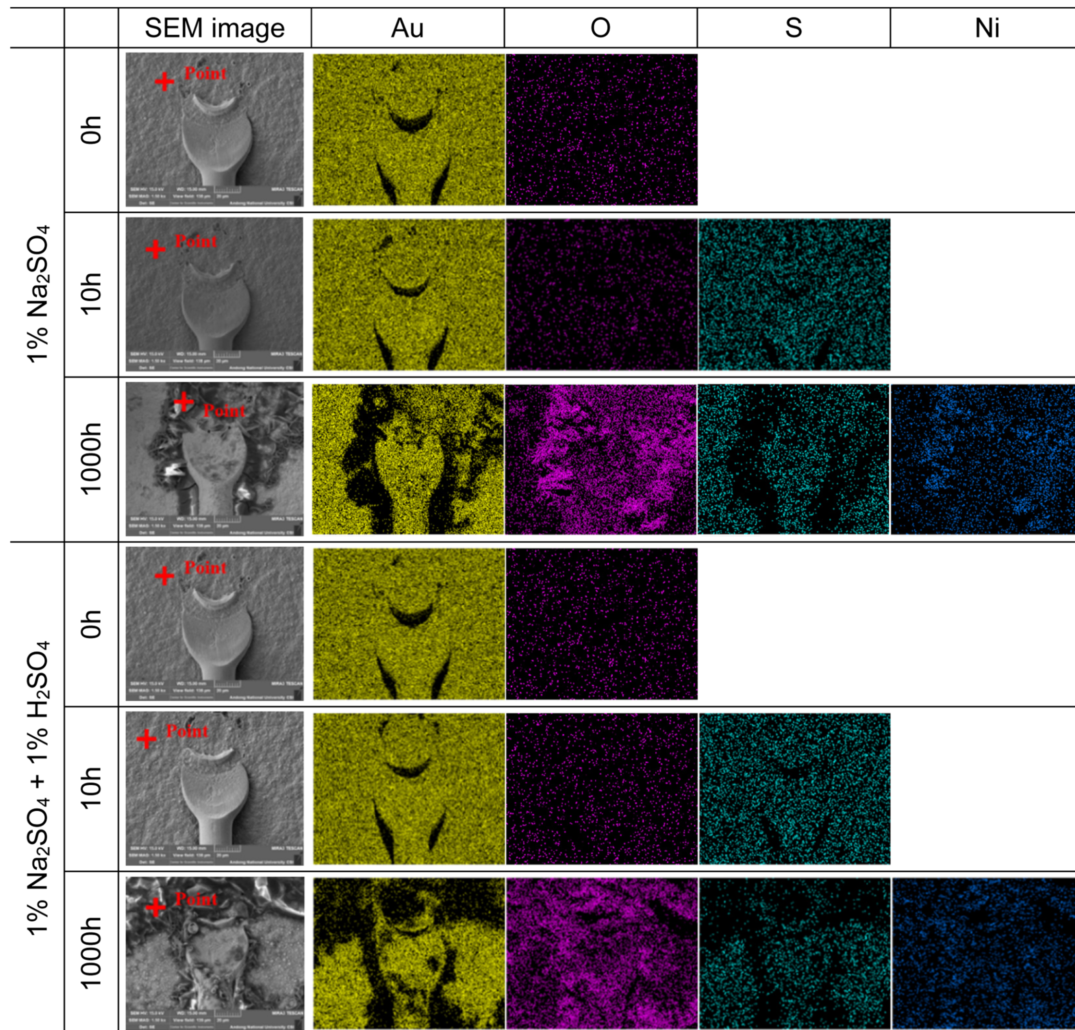

(a)

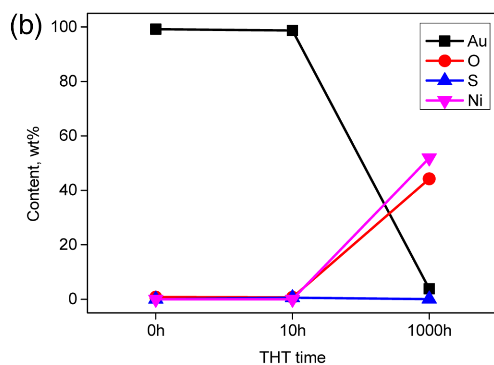

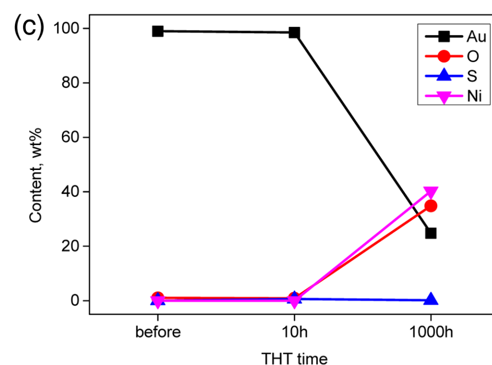

Fig. 9. Elemental distribution of 2nd stitch bond area of Au wire-bonded PCB unit by THT (Test chamber: 85 °C/85% RH, Test solution in corrosion cell: 1% Na_2SO_4 + x% H_2SO_4): (a) SEM image and EDS mapping, (b) Point analysis for 1% Na_2SO_4, (c) Point analysis for 1% Na_2SO_4 +1% H_2SO_4

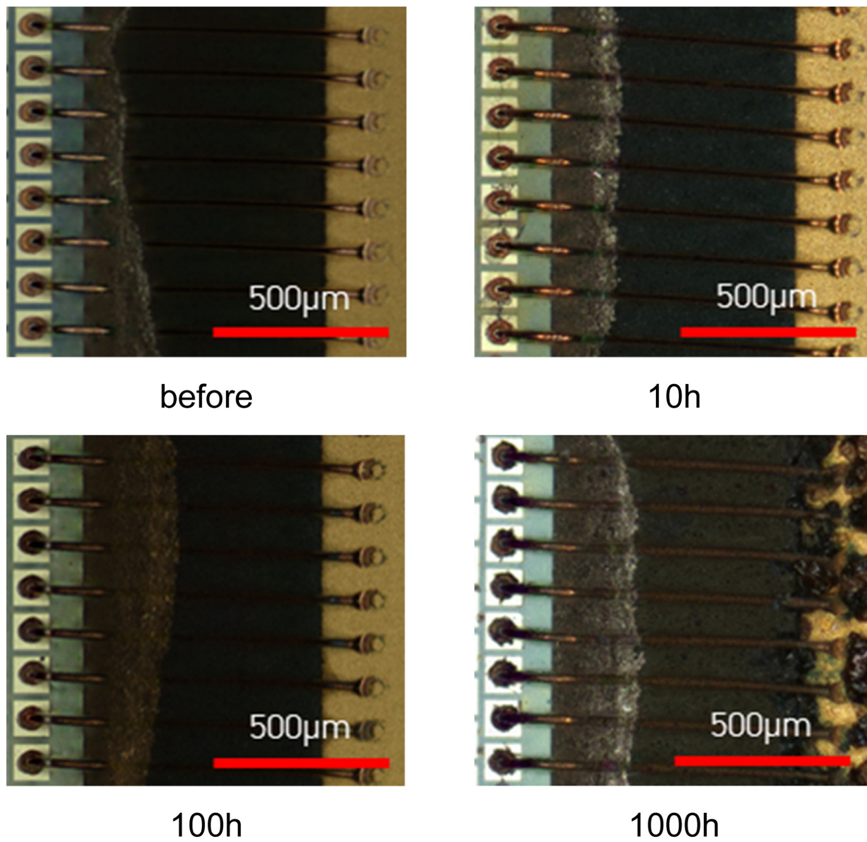

Fig. 10. Effect of test duration on corrosion appearance of Cu wire-bonded PCB unit by THT (Test chamber: 85 ºC/85% RH, Test solution in corrosion cell: 1% Na_2SO_4)

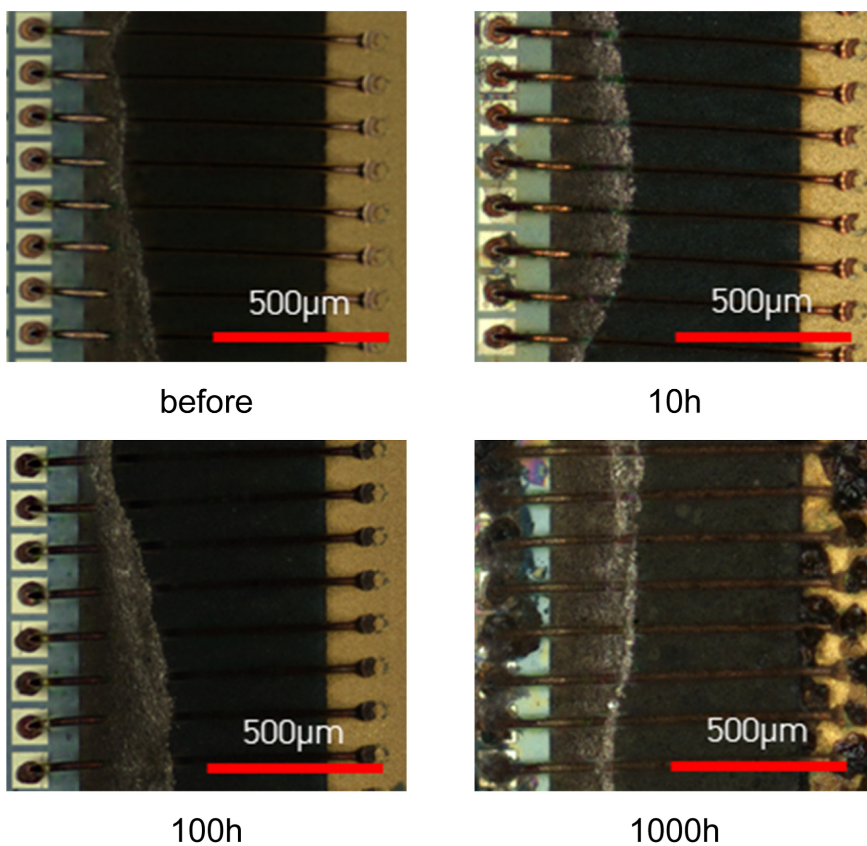

Fig. 11. Effect of test duration on corrosion appearance of Cu wire-bonded PCB unit by THT (85 ºC/ 85% RH): (a) 1% Na_2SO_4, (b) 1% Na_2SO_4 + 1% H_2SO_4

of localized Ni exposure at ENIG interfaces and the associated formation of Ni oxide [43-45].

Fig. 10 and Fig. 11 show the 3D microscopic observations of the Cu-wired unit. In 1% Na_2SO_4, small initial corrosion traces are observed at the edge of the ball bond after 10 h, and after 1000 h the entire ball bond region becomes darkened. In 1% Na_2SO_4 + 1% H_2SO_4, corrosion around the Al pad becomes evident from 10 h and propagates along the pad-

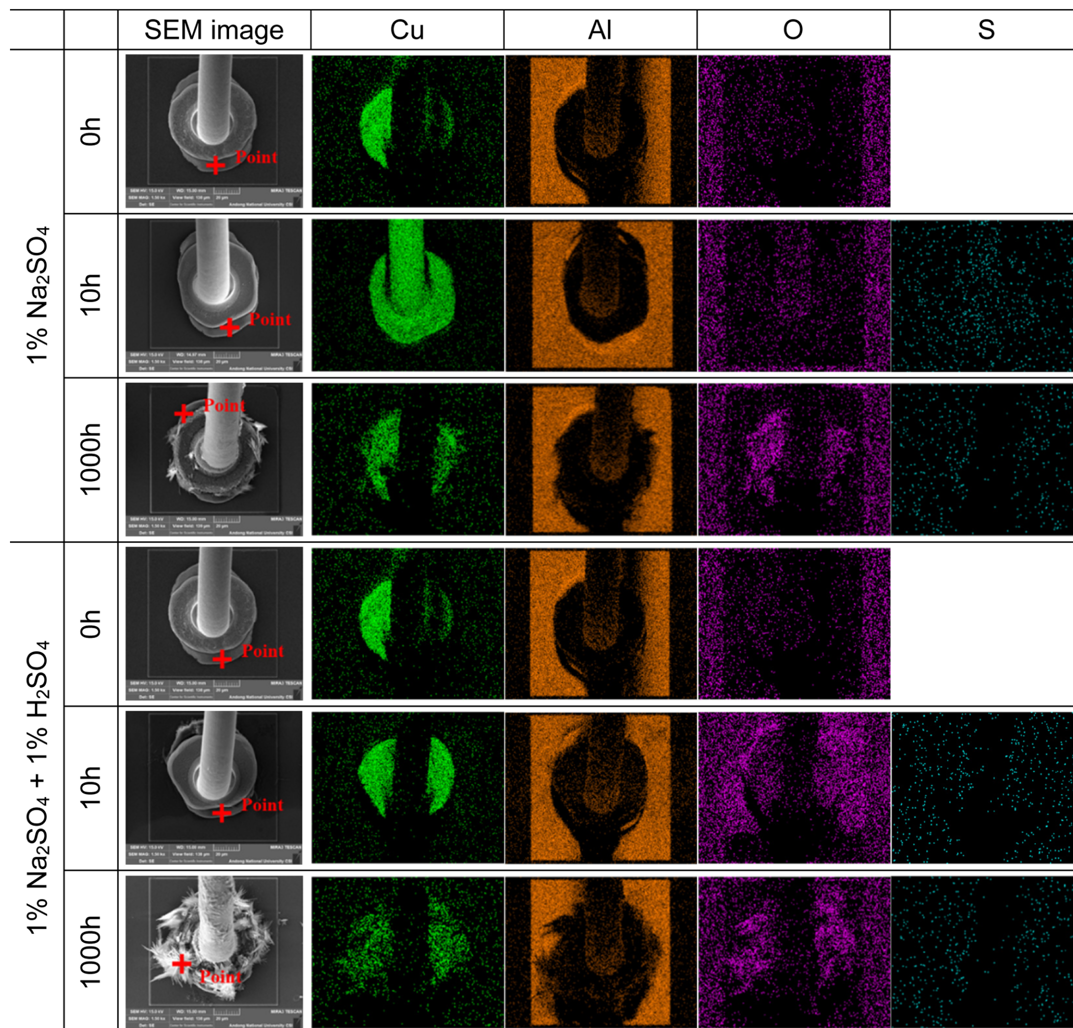

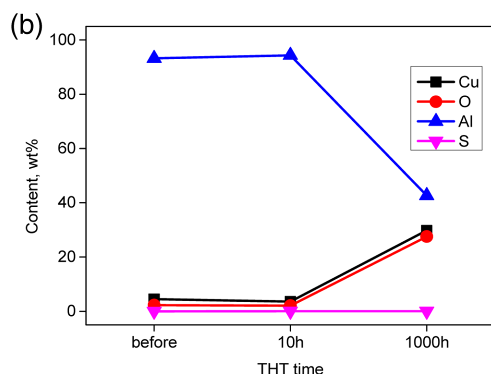

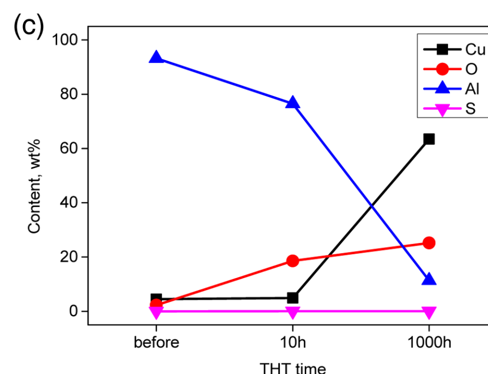

Fig. 12. Elemental distribution of 1st ball bond area of Cu wire-bonded PCB unit by THT (Test chamber: 85 °C/85% RH, Test solution in corrosion cell: 1% Na_2SO_4 + x% H_2SO_4): (a) SEM image and EDS mapping, (b) Point analysis for 1% Na_2SO_4, (c) Point analysis for 1% Na_2SO_4 + 1% H_2SO_4

ball interface. By 1000 h, both the ball bond and the Al pad are extensively covered with corrosion products. Meanwhile, the evolution of the external appearance of the 2nd stitch bond is similar to that observed for the Au-wired unit.

Fig. 12 shows the SEM-EDS elemental mapping and quantitative point-analysis results for the 1st ball bond of the Cu-wired unit. Compared with the initial (0 h) state, where the elemental distributions at the boundary between

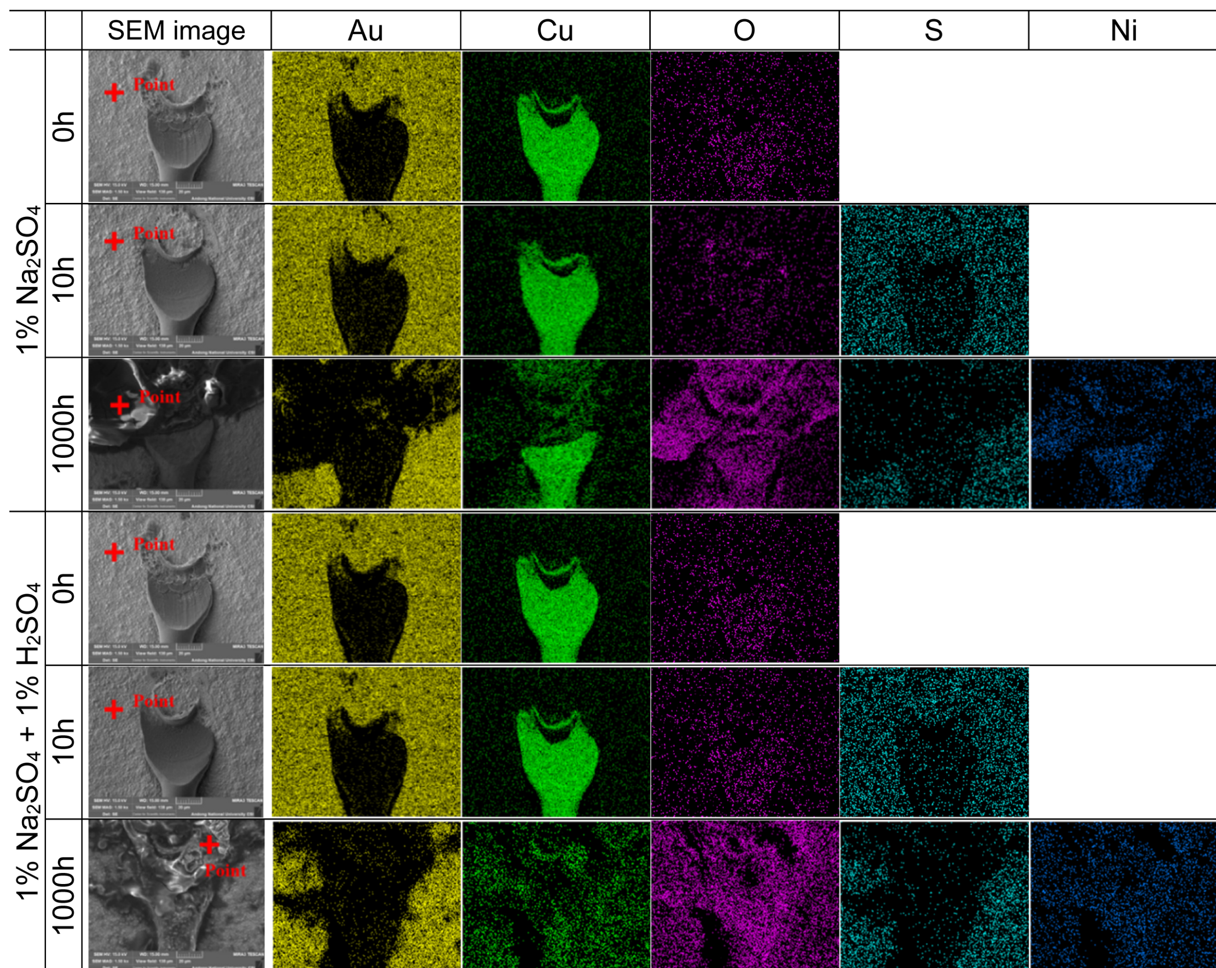

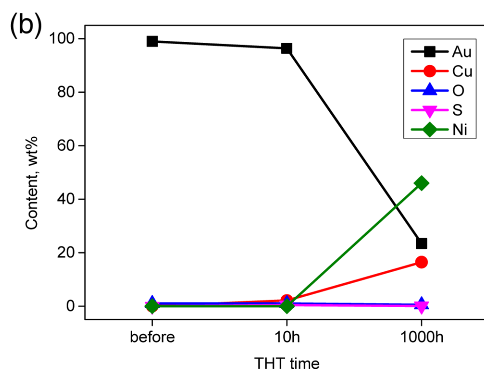

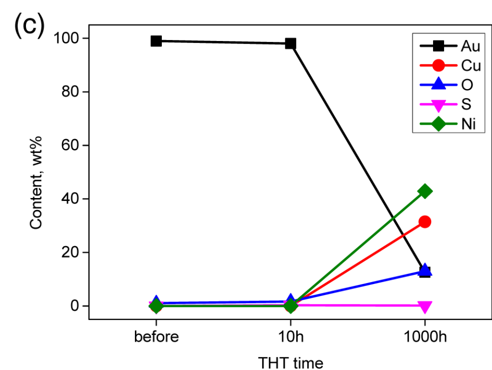

Fig. 13. Elemental distribution of 2nd stitch bond area of Cu wire-bonded PCB unit by THT (Test chamber: 85 °C/85% RH, Test solution in corrosion cell: 1% Na_2SO_4 + x% H_2SO_4): (a) SEM image and EDS mapping, (b) Point analysis for 1% Na_2SO_4, (c) Point analysis for 1% Na_2SO_4 + 1% H_2SO_4

the ball bond and Al pad are clearly defined, only minor changes in appearance are observed after 10 h in 1% Na_2SO_4, and the distributions of Al and Cu remain nearly unchanged. In contrast, in 1% Na_2SO_4 + 1% H_2SO_4, an increase in the O signal is detected in the Al region around the ball bond after 10 h. After 1000 h, both conditions exhibit a decrease in the Cu and Al signals, accompanied by a pronounced increase in the O signal. In addition, under the 1% Na_2SO_4 + 1% H_2SO_4 condition, the extent of corrosion is larger, and needle-like corrosion products are observed near the bonding interface. According to the point-analysis results, in 1% Na_2SO_4 a decrease in Al wt% and an increase in Cu and O wt% are only evident after 1000 h, whereas in 1% Na_2SO_4 + 1% H_2SO_4 a decrease in Al wt% and an increase in O wt% are already observed after 10 h. After 1000 h in the acidic solution, the Cu wt% is markedly higher and the Al wt% is markedly lower compared with the non-acidic condition. This time- and acidity-dependent behavior is consistent with previous reports that Cu-Al joints are particularly susceptible to corrosion in acidic environments [23].

Fig. 13 shows the surface morphology and EDS results for the 2nd stitch bond of the Cu-wired Unit. At 0 h, the stitch bond geometry is clearly defined, and the cutting mark left by severing the wire is distinct. Up to 10 h, no significant change in appearance is observed in either 1% Na_2SO_4 or 1% Na_2SO_4 + 1% H_2SO_4, although a slight increase in the O signal is detected around the stitch bond in the H_2SO_4-containing solution. After 1000 h, both conditions exhibit a decrease in the Cu signal and a pronounced increase in the O signal, with these changes being more evident in the acidic solution. At this stage, a Ni signal that had not been observed at earlier times also becomes evident. The point-analysis results likewise show little change up to 10 h in both solutions. After 1000 h, the Au wt% decreases markedly, while the Cu and Ni wt% increase under both conditions. In the acidic solution, a slight increase in O wt% is also observed. This behavior can be interpreted as concurrent local exposure of the underlying Ni layer at the ENIG interface and the associated formation of Ni oxide, consistent with previous reports [43-45].

Fig. 14 schematically illustrates the electrochemical corrosion mechanisms at the bond pad-wire interface based on the above results. In the 1st ball bond of the Au-wired unit, the potential difference between Au and Al drives galvanic dissolution of the Al pad, and the resulting Al-based oxygen-enriched corrosion products (e.g., CuO,

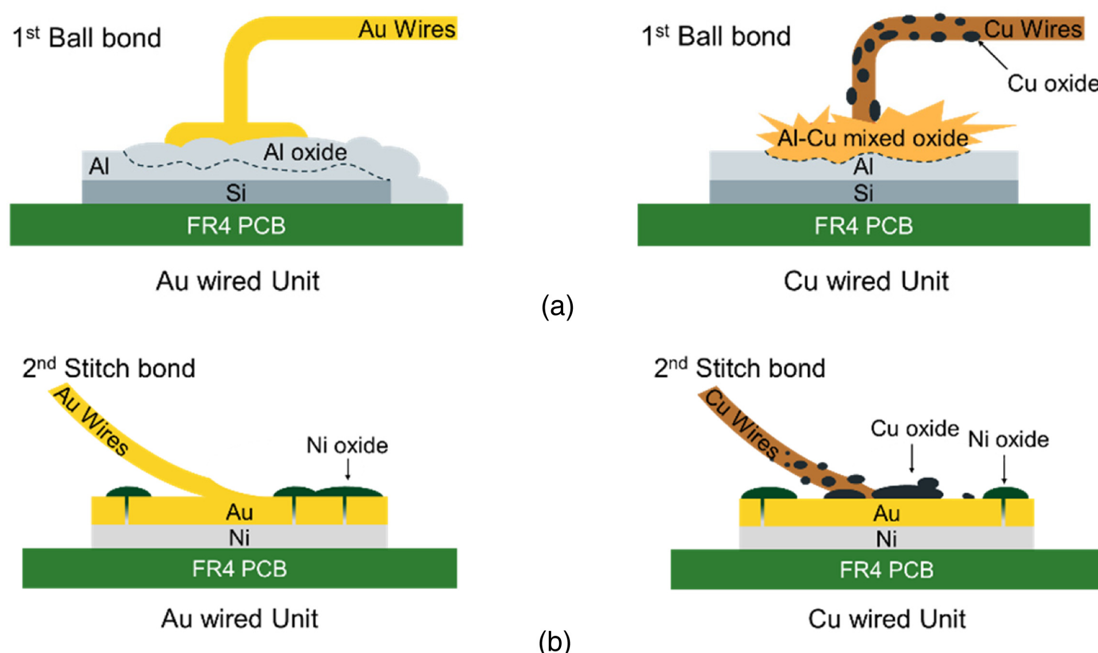

Fig. 14. Comparison of corrosion model between Au wire and Cu wire bonded PCB unit by THT in 1% Na_2SO_4 + 1% H_2SO_4: (a) 1st ball bond area, (b) 2nd stitch bond area

Cu_2O, Al_2O_3, Cu_2S, CuS, Al_2S_3) subsequently form a layer that covers the pad surface. In contrast, in the Cu-wired unit, pad-side Al dissolution is accompanied by independent corrosion of Cu. As a result, dark Cu-containing oxygen-enriched corrosion products (e.g., CuO, Cu_2O, Al_2O_3, Cu_2S, CuS, Al_2S_3) form around the wire, while mixed Al-Cu oxygen-enriched corrosion products (e.g., CuO, Cu_2O, Al_2O_3, Cu_2S, CuS, Al_2S_3) grow in a needle-like morphology along the bonding interface [46,47].

For the 2nd stitch bond in the Au-wired unit, even though the wire and pad are both Au, microscopic defects in the Au plating allow the underlying Ni layer to become locally exposed, accompanied by the formation of Ni oxide [43-45]. In the Cu-wired unit, corrosion of the Cu wire leads to the formation of oxygen-enriched corrosion products (e.g., CuO, Cu_2O, Al_2O_3, Cu_2S, CuS, Al_2S_3) on the wire surface [29]. In parallel, localized exposure of the Ni layer can occur with Ni oxide, such that both Cu and Ni oxide [43-45].

4. Conclusions

This study investigated the influence of sulfuric acid concentration on the corrosion behavior at packaging-relevant Al and Au pad-Au and Cu wire interfaces by means of electrochemical tests and a Temperature-Humidity Test (THT). The main conclusions are as follows.

Polarization tests revealed that the corrosion rate increased in the order Au wire < sputtered Al < Cu wire. The galvanic corrosion rate of Al in the Au-Al couple was higher than that in the Cu-Al couple. This is attributed to the larger potential difference (ΔE) of the Au-Al pair and the cathodic Tafel behavior of Au.

After the THT (85 °C/85% RH), macroscopic observations showed that the Cu-wired unit exhibited more severe corrosion than the Au-wired unit, with extensive attack of the 1st ball bond and the wire. This indicates that the intrinsic corrosion tendency of Cu in the sulfate-based environment dominated over the galvanic effect, so that the actual corrosion of the Cu wire was more severe than would be predicted from galvanic considerations alone.

In the Au pad of the 2nd stitch bond, corrosion products enriched in Ni and O were detected, which is interpreted as a result of deterioration due to local exposure of the lower Ni layer through micro-defects in the ENIG structure [43-45]. In addition, in the 2nd stitch bond of the Cu-wired unit, the O signal increased along with a decrease in the Cu signal, suggesting that oxygen-enriched corrosion products (e.g., CuO, Cu_2O, Al_2O_3, Cu_2S, CuS, Al_2S_3) were also formed on the Cu surface.

Acknowledgement

This work was supported by Korea Institute for Advancement of Technology (KIAT) grant funded by the Korea Government (MOTIE) (RS-2024-00409639, HRD Program for Industrial Innovation). The authors would like to thank MK electron Co., Ltd., for supplying the materials.

References

1. G. G. Harman, *Wire Bonding in Microelectronics*, *3re ed.*, p. 1, McGraw-Hill, New York (2010).
2. H. Zhou, Y. Zhang, J. Cao, C. Su, C. Li, A. Chang, and B. An, Research Progress on Bonding Wire for Microelectronic Packaging, *Micromachines*, **14**, 432 (2023). Doi: https://doi.org/10.3390/mi14020432
3. R. R. Tummala, *Fundamentals of Microsystems Packaging*, *2nd ed.*, p. 311, McGraw-Hill, New York (2008).
4. H. K. Kung, H. S. Chen, and M. C. Lu, The Wire Sag Problem in Wire Bonding Technology for Semiconductor Packaging, *Microelectronics Reliability*, **53**, 288 (2013). Doi: https://doi.org/10.1016/j.microrel.2012.08.017
5. Y. Zhang, H. Guo, J. Cao, X. Wu, H. Jia and A. Chang, Research Progress of Palladium-Plated Copper Bonding Wire in Microelectronic Packaging, *Micromachines*, **14**, 1538 (2023). Doi: https://doi.org/10.3390/mi14081538
6. B. An, H. Zhou, J. Cao, P. Ming, J. Persic, J. Yao, A. Chang, A Review of Silver Wire Bonding Techniques, *Micromachines*, **14**, 2129 (2023). Doi: https://doi.org/10.3390/mi14112129
7. C. S. Goh, Y. L. E. Chong, T. K. Lee and C. Breach, Corrosion Studies and Intermetallic Formation in Gold and Copper Bonding in Microelectronics Packaging, *Crystals*, **3**, 391 (2013). Doi: https://doi.org/10.3390/cryst3030391
8. C. D. Breach and F. Wulff, New Observations on Inter Metallic Compound Formation in Gold Ball Bonds: General Growth Patterns and Identification of Two Forms of Au_4Al, *Microelectronics Reliability*, **44**, 973 (2004). Doi:

https://doi.org/10.1016/j.microrel.2004.02.013

9. G. G. Harman and C. L. Wilson, Materials Problems Affecting Reliability and Yield of Wire Bonding in VLSI Devices, *MRS Online Proceedings Library*, **154**, 401 (1989). Doi: https://doi.org/10.1557/PROC-154-401
10. H. Xu, C. Liu, V. V. Silberschmidt, S. S. Pramana, T. J. White, Z. Chen, and V. L. Acoff, New Mechanisms of Void Growth in Au-Al Wire Bonds: Volumetric Shrinkage and Intermetallic Oxidation, *Scripta Materialia*, **65**, 642 (2011). Doi: https://doi.org/10.1016/j.scriptamat.2011.06.050
11. A. Teverovsky, *Proc. IEEE Int. Reliability Physics Symposium*, p. 547, IEEE, Phoenix, AZ, USA (2004). Doi: https://doi.org/10.1109/RELPHY.2004.1315388
12. P. Chauhan, Z. W. Zhong, and M. Pecht, Copper Wire Bonding Concerns and Best Practices, *Journal of Electronic Materials*, **42**, 2415 (2013). Doi: https://doi.org/10.1007/s11664-013-2576-1
13. Z. W. Zhong, Wire bonding using copper wire, *Microelectronics International*, **26**, 10 (2009). Doi: https://doi.org/10.1108/13565360910923115
14. H. J. Kim, J. Y. Lee, K. W. Paik, K. W. Koh, J. Won, S. Choe, J. Lee, J. T. Monn, and Y. J. Park, Effects of Cu/Al Intermetallic Compound (IMC) on Copper Wire and Aluminum Pad Bondability, *IEEE Transactions on Components and Packaging Technologies*, **26**, 367 (2003). Doi: https://doi.org/10.1109/TCAPT.2003.815121
15. C. Papadopoulos, T. Villiger, S. Steiner, J. Prinz, C. Morabito, M. Cammarata, A. Rodriguez, J. Kwon, R. Geilenkeuser, D. Breuer, F. Kuechenmeister, J. Dienelt, J. Urban, H. Kabus and J. Krinke, Gold Wire Bond Study for Automotive Application, *Microelectronics Reliability*, **114**, 113899 (2020). Doi: https://doi.org/10.1016/j.microrel.2020.113899
16. AEC-Q100 Rev. J, Failure Mechanism Based Stress Test Qualification for Integrated Circuits (2023).
17. ISO 16750-4, Road vehicles—Environmental conditions and testing for electrical and electronic equipment—Part 4: Climatic loads (2010).
18. JESD22-A101D, Steady-State Temperature Humidity Bias Life Test (2015).
19. T. K. Lee, C. D. Breach, W. L. Chong, and C. S. Goh, *Proceedings of the International Conference on Electronic Packaging Technology & High Density Packaging,* p. 163, IEEE, Guilin, China (2012).
20. H. Fu, C. Chen, P. Singh, J. Zhang, A. Kurella, X. Chen, X. Jiang, J. Burlingame, and S. Lee, *Proceedings of the SMTA Pan Pacific Microelectronics Symposium*, p. 1, SMTA, Kauai, HI, USA (2012).
21. D. W. Rice, P. Peterson, E. B. Rigby, P. B. P. Phipps, R. J. Cappell, and R. Tremoureux, Atmospheric Corrosion of Copper and Silver, *Journal of The Electrochemical Society*, **128**, 275 (1981). Doi: https://doi.org/10.1149/1.2127403
22. T. T. M. Tran, C. Fiaud, and E. M. M. Sutter, Oxide and Sulphide Layers on Copper Exposed to H_2S Containing Moist Air, *Corrosion Science*, **47**, 1724 (2005). Doi: https://doi.org/10.1016/j.corsci.2004.08.019
23. C. W. Tan, A. R. Daud, and M. A. Yarmo, Corrosion Study at Cu-Al Interface in Microelectronics Packaging, *Applied Surface Science*, **191**, 67 (2002). Doi: https://doi.org/10.1016/S0169-4332(02)00150-2
24. W. Qin, H. Anderson, T. Anderson, G. Chang, and D. Barrientos, Proc. *IEEE Electronic Components and Technology Conference*, p. 1, IEEE, San Diego, CA (2018). Doi: https://doi.org/10.1109/ECTC.2018.00221
25. Y. Wu, S. Calabrese Barton, and A. Lee, Galvanic Corrosion Behavior at the Cu-Al Ball Bond Interface: Influence of Pd Addition and Chloride Concentration, *Microelectronics Reliability*, **92**, 79 (2019). Doi: https://doi.org/10.1016/j.microrel.2018.11.016
26. N. Ross, M. Asokan, G. I. Ashok Kumar, J. Caperton, J. Alptekin, A. S. Salunke, and O. M. Chyan, Mechanistic Study of Copper Wire-Bonding Failures on Packaging Devices in Acidic Chloride Environments, *Microelectronics Reliability*, **113**, 113917 (2020). Doi: https://doi.org/10.1016/j.microrel.2020.113917
27. Y. R. Yoo, G. Kim, S. M. Jeon, H. J. Park, W. W. Seo, J. T. Moon, and Y. S. Kim, Influence of HCl Concentration on Corrosion Behavior between Au or Cu Bonding Wires and the Bond Pad for Semiconductor Packaging, Materials, **16**, 7275 (2023). Doi: https://doi.org/10.3390/ma16237275
28. G. I. Ashok Kumar, A. Lambert, J. Caperton, M. Asokan, W. Yi, and O. Chyan, Comparative Study of Chloride and Fluoride Induced Aluminum Pad Corrosion in Wire-Bonded Device Packaging Assembly, *Corrosion and Materials Degradation*, **2**, 447 (2021). Doi: https://doi.org/10.3390/cmd2030023
29. M. Asokan, J. Caperton, A. Salunke, O. Chyan, and F. Xu, Bond Reliability Under Humid Environment for Coated Copper Wire and Bare Copper Wire, *Microelectronics Reliability*, **51**, 148 (2010). Doi: https://doi.org/10.1016/j.microrel.2010.03.006
30. A. Mavinkurve, L. Goumans, M. L. Farrugia, E. van Olst, M. van Soestbergen, R. T. H. Rongen, and B. Bumrungkittikul, *Proc. IEEE 67th Electronic Components and Technology Conf. (ECTC)*, p. 1171, IEEE, Orlando,

FL (2017). Doi: https://doi.org/10.1109/ECTC.2017.252

31. F. C. Walsh and C. Ponce de León, Versatile Electrochem Ical Coatings and Surface Layers from Aqueous Methane Sulfonic Acid, *Surface and Coatings Technology*, **259**, 676 (2014). Doi: https://doi.org/10.1016/j.surfcoat.2014.10.010
32. M. V. Soestbergen, P. M. Biesheuvel, R. T. H. Rongen, L. J. Ernst and G. Q. Zhang, Modified Poisson-Nernst-Planck Theory for Ion Transport in Polymeric Electrolytes, *Journal of Electrostatics*, **66**, 567 (2008). Doi: https://doi.org/10.1016/j.elstat.2008.06.005
33. A. A. Omar, A. Jalar, M. Abu Bakar, and K. Abdul Hamid, Sulfur Ingression on Encapsulated Leadframe of Discrete Semiconductor Package, *IEEE Transactions on Components, Packaging and Manufacturing Technology*, **12**, 544 (2022). Doi: https://doi.org/10.1109/TCPMT.2022.3149521
34. IPC 4101, Specification for Base Materials for Rigid and Multilayer Printed Boards (2017).
35. ASTM G5-94(2004), Standard Reference Test Method for Making Potentiostatic and Potentiodynamic Anodic Polarization Measurements (2004).
36. ASTM G102(2004), Standard Practice for Calculation of Corrosion Rates and Related Information from Electrochemical Measurements (2004).
37. IUPAC, *Compendium of Chemical Terminology*, *2nd ed.*, p. 59, standard electrode potential, E° (1997). Doi: https://doi.org/10.1351/goldbook.S05912
38. KS D 0277, Standard guide for conducting and evaluating galvanic corrosion tests in electrolytes (2005).
39. W. C. Moshier, G. D. Davis, and J. S. Ahearn, The Corrosion and Passivity of Aluminum Exposed to Dilute Sodium Sulfate Solutions, *Corrosion Science*, **27**, 785 (1987). Doi: https://doi.org/10.1016/0010-938X(87)90037-0
40. A. Kolics and A. Wieckowski, Adsorption of Sulfate and Chloride Ions on Aluminum, *Electrochimica Acta*, **43**, 2605 (1998). Doi: https://doi.org/10.1016/S0013-4686(97)10188-8
41. R. W. Revie (ed.), *Uhlig's Corrosion Handbook*, *3rd ed.*, p. 234, Wiley, Hoboken, NJ (2011). Doi: https://doi.org/10.1002/9780470872864
42. M. Pourbaix, *Atlas of Electrochemical Equilibria in Aqueous Solutions*, *2nd ed.*, p. 170, NACE International, Houston, TX (1974).
43. E. Salahinejad, R. Eslami Farsani, and L. Tayebi, Synergistic Galvanic-Pitting Corrosion of Copper Electrical Pads Treated with Electroless Nickel-Phosphorus/Immersion Gold Surface Finish, *Engineering Failure Analysis*, **77**, 138 (2017). Doi: https://doi.org/10.1016/j.engfailanal.2017.03.001
44. E. F. Monlevade, I. A. P. Cardoso, E. F. L. Maciel, and N. Alonso-Falleiros, Galvanic Corrosion of Electroless Nickel/ Immersion Gold Plated Non-Permanent Electric Contacts Used in Electronic Devices-Direct Evidence of Triggering Mechanism, *Engineering Failure Analysis*, **96**, 562 (2019). Doi: https://doi.org/10.1016/j.engfailanal.2018.12.001
45. M. Mousavi, A. Kosari, J. M. C. Mol, and Y. Gonzalez-Garcia, Localised Aqueous Corrosion of Electroless Nickel Immersion Gold-Coated Copper, *Corrosion Engineering, Science and Technology*, **57**, 520 (2022). Doi: https://doi.org/10.1080/1478422X.2022.2096322
46. H. Kwon and N. Cho, Corrosion Behaviors of Outdoor Bronze Sculptures in an Urban-Industrial Environment: Corrosion Experiment on Artificial Sulfide Patina, *Metals*, **13**, 1101 (2023). Doi: https://doi.org/10.3390/met13061101
47. M. Abdelbar and A. M. El-Shamy, Understanding Soil Factors in Corrosion and Conservation of Buried Bronze Statuettes: Insights for Preservation Strategies, *Scientific Reports*, **14**, 19230 (2024). Doi: https://doi.org/10.1038/s41598-024-69490-5
48. Z. Ghelichkhah, D. D. Macdonald, and G. S. Ferguson, Mechanistic Analysis of Hydrogen Evolution Reaction on Stationary Polycrystalline Gold Electrodes in H_2SO_4 Solutions, *Corrosion and Materials Degradation*, **5**, 241 (2024). Doi: https://doi.org/10.3390/cmd5020010
49. S. Behjati and M. T. M. Koper, In Situ STM Study of Roughening of Au(111) Single-Crystal Electrode in Sulfuric Acid Solution during Oxidation-Reduction Cycles, *The Journal of Physical Chemistry C*, **128**(44), 19024 (2024). Doi: https://doi.org/10.1021/acs.jpcc.4c06362
50. T. Munson, Failure Analysis - Using Ion Chromatography and Ion Chromatography/Mass Spec (IC/MS), SMTA Pan Pac Conference 2020 - Foresite Inc (2020).
51. P. Arellanes-Lozada, O. Olivares-Xometl, D. Guzmán-Lucero, N. V. Likhanova, M. A. Domínguez-Aguilar, I. V. Lijanova, E. Arce-Estrada, The Inhibition of Aluminum Corrosion in Sulfuric Acid by Poly(1-vinyl-3-alkyl-imidazolium Hexafluorophosphate), *Materials*, **7**, 5711 (2014). Doi: https://doi.org/10.3390/ma7085711
52. O. Adel, M. E. Mohamed, and E. Khamis, Thermodynamic, Electrochemical and Surface Characterization of Copper Corrosion Inhibition in Acidic Solution Using Rice Straw Extract, *Scientific Reports*, **15**, 27753 (2025). Doi: https://doi.org/10.1038/s41598-025-12482-w